



Contents lists available at ScienceDirect

Remote Sensing of Environment

journal homepage: www.elsevier.com/locate/rse

Integrating multi-temporal spectral and structural information to map wetland vegetation in a lower Connecticut River tidal marsh

Martha S. Gilmore^{a,*}, Emily H. Wilson^b, Nels Barrett^c, Daniel L. Civco^d, Sandy Prisloe^b, James D. Hurd^d, Cary Chadwick^b

^a Department of Earth and Environmental Sciences, Wesleyan University, 265 Church St., Middletown CT 06459, United States

^b Center for Land Use Education and Research (CLEAR), Department of Extension, College of Agriculture and Natural Resources, University of Connecticut, 1066 Saybrook Road, PO Box 70, Haddam CT 06438, United States

^c U.S. Department of Agriculture, Natural Resources Conservation Service, 344 Merrow Road, Suite A, Tolland CT 06084, United States

^d Center for Land Use Education and Research (CLEAR), Department of Natural Resources Management and Engineering, College of Agriculture and Natural Resources, University of Connecticut, Box U-4087, Room 308, 1376 Storrs Road, Storrs CT 06269, United States

ARTICLE INFO

Article history:

Received 1 June 2007

Received in revised form 18 April 2008

Accepted 3 May 2008

Available online xxxx

Keywords:

Coastal wetlands

Image classification

LiDAR

Phragmites australis

QuickBird

Spectroradiometer

Vegetation monitoring

ABSTRACT

This study examines the effectiveness of using multi-temporal satellite imagery, field spectral data, and LiDAR top of canopy data to classify and map the common plant communities of the Ragged Rock Creek marsh, located near the mouth of the Connecticut River. Visible to near-infrared (VNIR) reflectance spectra were measured in the field over the 2004–2006 growing seasons to assess the phenological variability of the dominant marsh plant species, *Spartina patens*, *Phragmites australis* and *Typha* spp. *Phragmites* was best distinguished from other species by its high NIR response late in the growing season. *Typha* spp. had a high red/green ratio and *S. patens* had a unique green/blue ratio relative to other species throughout the bulk of the growing season. The field spectra and single date (2004) LiDAR canopy height data were used to define an object-oriented classification methodology for the three plant communities in multi-temporal QuickBird multispectral imagery collected over the same time interval. The classification was validated using an extensive field inventory of marsh species. Overall maximum fuzzy accuracy for the classification was 97% for *Phragmites*, 63% for *Typha* spp. and 80% for *S. patens* meadows and improved to 97%, 76%, and 92%, respectively, using a fuzzy acceptable match measure. This study demonstrated the importance of the timing of image acquisition for the identification of targeted plant species in a heterogeneous marsh. These datasets and protocols may provide coastal resource managers, municipal officials and researchers a set of recommended guidelines for remote sensing data collection for marsh inventory and monitoring.

© 2008 Elsevier Inc. All rights reserved.

1. Introduction

Coastal wetlands are a critical and dynamic component of the Long Island Sound ecosystem. Over the past century, a significant amount of these wetlands has been lost due to development, filling and dredging, or damaged due to anthropogenic disturbance and modification. Global sea level rise is also likely to have a significant impact on the condition and health of coastal wetlands, particularly if the wetlands cannot migrate due to dense coastal development (e.g., Donnelly & Bertness, 2001). In addition to physical loss of marshes, the species composition of marsh communities is changing. *Spartina alterniflora* (saltwater cordgrass) and *Spartina patens* (salt meadow grass), once the dominant

species of New England salt marshes, are being replaced by monocultures of the non-native genotype of *Phragmites australis* (Cav.) Trin. ex Steud (common reed) in Connecticut marshes (Barrett & Prisloe, 1998; Chambers et al., 1999; Orson, 1999; Warren et al., 2001). *Phragmites* outcompetes other marsh species in areas with increased fresh water, nitrogen and sediment and its presence is positively correlated with marsh fragmentation (Moore et al., 1999; Bertness et al., 2002; Bart et al., 2006). In response to the increase of *Phragmites* in many marshes, several government agencies, academic institutions, and conservation organizations have instituted efforts (commencing in the 1980s) to restore marsh health, including the eradication of *Phragmites* in some areas. The response of marshes to eradication includes both an increase of non-*Phragmites* marsh species and *Phragmites* reinvasion (Farnsworth & Meyerson, 1999; Meyerson et al., 2000).

With the mounting anthropogenic and climatic pressures on coastal wetland areas, it is becoming increasingly important to identify and inventory the current extent and condition of wetlands located throughout the coastal region of the Long Island Sound estuary, implement a cost effective method to track changes in the condition of

* Corresponding author.

E-mail addresses: mgilmore@wesleyan.edu (M.S. Gilmore), emily.wilson@uconn.edu (E.H. Wilson), nels.barrett@ct.usda.gov (N. Barrett), daniel.civco@uconn.edu (D.L. Civco), sandy.prisloe@uconn.edu (S. Prisloe), james.hurd_jr@uconn.edu (J.D. Hurd), cary.chadwick@uconn.edu (C. Chadwick).

wetlands over time, and monitor the effects of habitat restoration and management activities. Because marsh fieldwork is labor intensive, remote sensing is an efficient way to characterize coastal wetlands due to its synoptic coverage and repeatability. For management applications, image data must be of high enough spatial and spectral resolution to effectively identify stands of each species without being cost-prohibitive. This has led many workers to develop classification methods using widely available high spatial resolution, low spectral resolution image data such as aerial photographs (e.g., Shima et al., 1976; Phinn et al., 1999; Shuman & Ambrose, 2003; Maheu-Giroux &

Blois, 2005) or to use coarse-resolution (30m–1km) multispectral data (e.g., Donoghue & Shennan, 1987; Arzandeh & Wang, 2003). These methods are most successful at identifying large-scale stands of dense, monotypical species, but have limited applicability to meter-scale mapping of individual species within a heterogeneous mosaic of marsh plants. Improved vegetation maps have been produced using traditional supervised and unsupervised classifiers on high spatial resolution multispectral and hyperspectral data (e.g., Underwood et al., 2003; Schmidt et al., 2004; Belluco et al., 2006; Wang et al., 2007; Pengra et al., 2007; Sadro et al., 2007; Laba et al., 2008). These

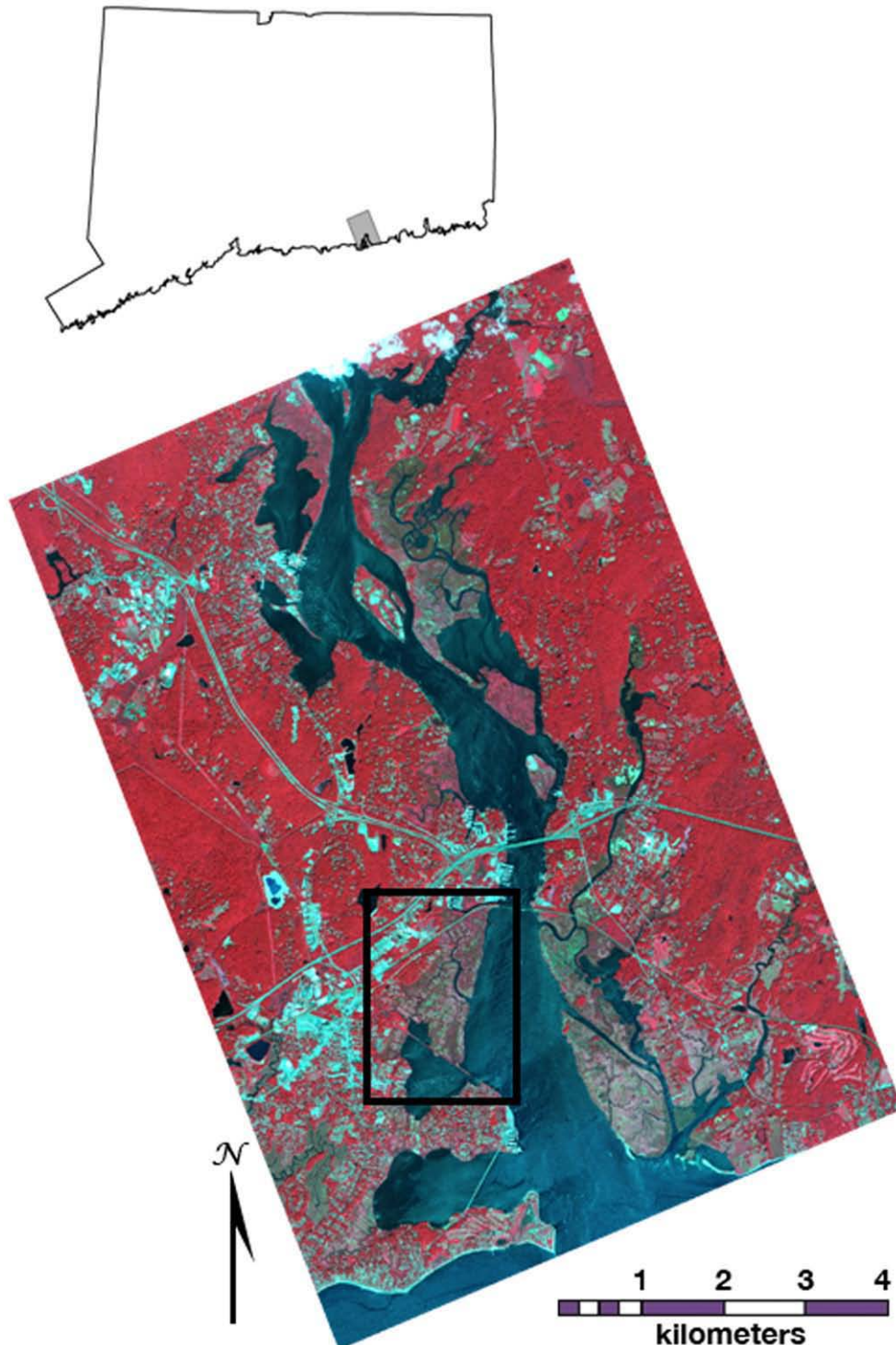


Fig. 1. Location of Ragged Rock Creek marsh, Old Saybrook, Connecticut. July 20, 2004 4-2-1 QuickBird image of the mouth of the CT River, inset refers to location of study site in Fig. 2.

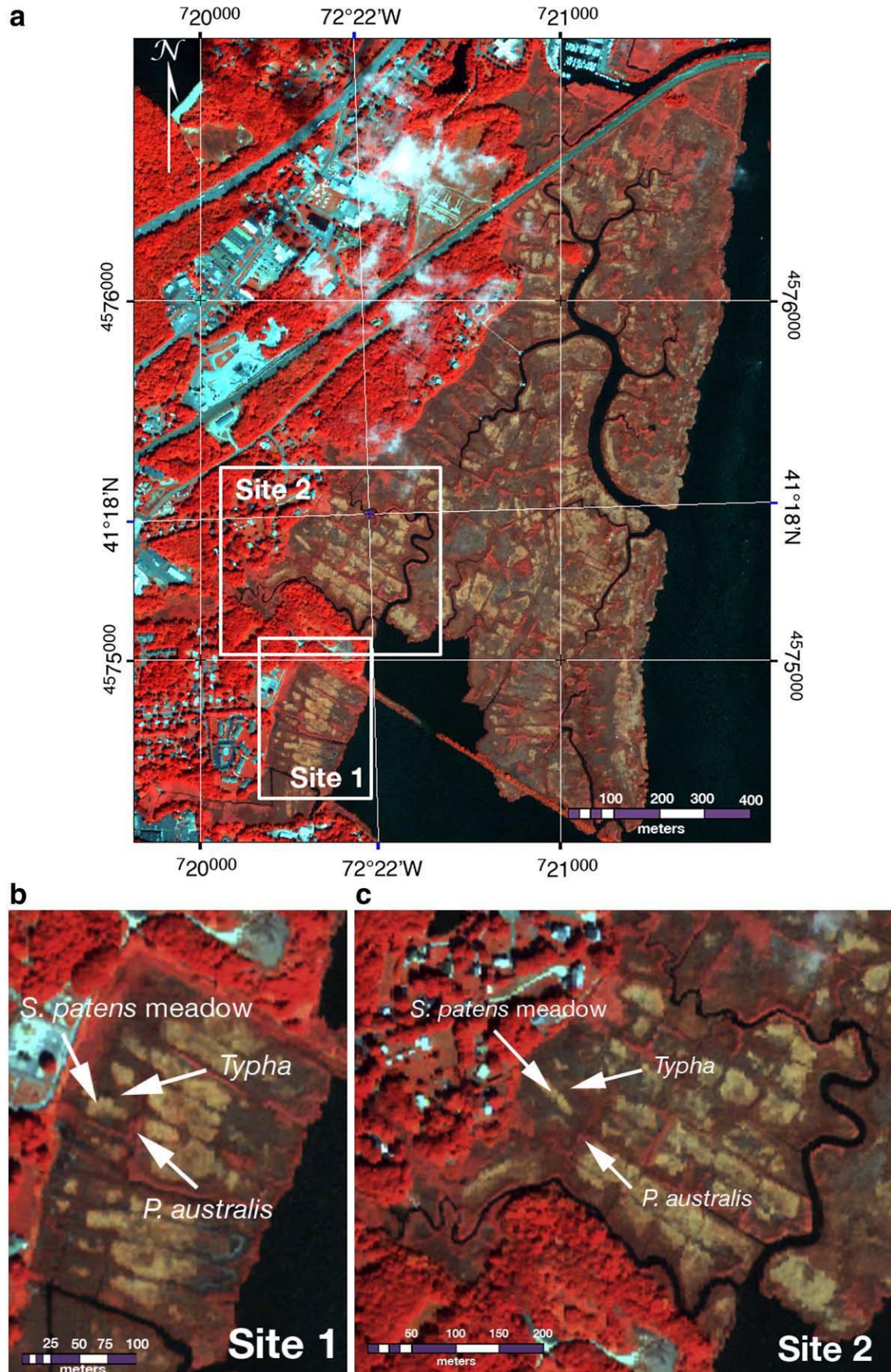


Fig. 2. September 12, 2004 4-2-1 QuickBird image of Ragged Rock Creek marsh, (a) overview of marsh, (b) Site 1, and (c) Site 2. Arrows indicate approximate areas where reflectance spectra were measured in the field throughout the growing season. Spectra were measured at Site 1 in 2004 and Site 2 in 2005 and 2006.

classification methodologies are based on image and/or ground reference data measured on a single date, which limits their applicability to images taken at other times. Vegetation phenology has long been recognized to be useful in discriminating species for vegetation mapping (e.g., Reed et al., 1994; Key et al., 2001), as the spectrum of a single species may vary throughout the growing season due to variations in the amount and ratios of plant pigments, leaf water content, plant height, canopy effects, leaf angle distribution and other structural characteristics. Previous work on the classification of marsh vegetation using multi-temporal image data (Dennison & Roberts, 2003; Belluco et al., 2006; Judd et al., 2007) and LiDAR data (Rosso et al., 2006) relies on judicious identification of endmembers, often derived from extensive field measurements. Such field measurements may be impractical if a goal is to inventory vegetation in even a small number of marshes. Endmember selection can be enhanced using image processing algorithms (e.g., Dennison & Roberts, 2003; Judd et al., 2007). In this work, we take a different approach, and test a new method to relate field measurements at a limited number of sites to image classification of an entire marsh.

Several studies demonstrate significant spectral differences between marsh plant species in both field reflectance data (Hardisky et al., 1986; Zhang et al., 1997; Schmidt & Skidmore, 2003; Gao & Zhang, 2006) and hyperspectral (Gross & Klemas, 1986) reflectance data at various times during the growing season. Laba et al. (2005) computed the derivatives of field reflectance spectra of purple loosestrife, *Phragmites* and cattail in the Hudson River estuary weekly throughout the growing season and determined that these species were best differentiated in late August. Artigas and Yang (2005) measured reflectance spectra of *Phragmites* in the field throughout the growing season and determined that the spectra were significantly separable, and that characteristics of the field spectra correlated with seasonal patterns of vigor interpreted from classified hyperspectral AISA data of the New Jersey Meadowlands. The results of these studies suggest that phenological variability of the VNIR reflectance of marsh plants can guide image classification, however none of these studies do so.

The purpose of this study was to propose and evaluate a novel approach, where characteristics of field reflectance spectra of marsh vegetation measured over the growing season were used to direct the classification of high spatial resolution multi-temporal QuickBird data (2.4m/pixel) of a Connecticut marsh. This is the first known attempt to use field reflectance characteristics to define rules for the classification of multi-temporal image data. Single date LiDAR data also contributed to the classification. Our goals were to: 1) determine the optimal times during the growing season for the discrimination of individual marsh plant species based on spectral reflectance and structure measured in the field, and 2) assess the utility of these field data to direct the classification of multi-temporal, multispectral images of the entire marsh, with particular attention to the mapping of the invasive species *Phragmites*. Additionally, we sought to provide mapping protocols that can be used to identify a single species, such as *Phragmites*, from a single date of multispectral imagery, as these data are likely to be the most accessible to land managers.

2. Study site

Ragged Rock Creek marsh is a 142-hectare brackish tidal marsh located on the western bank of the Connecticut River, approximately 2.5km north of its confluence with Long Island Sound (Fig. 1). The vegetation at Ragged Rock Creek marsh is typical of Connecticut's estuarine tidal marshes, where the pattern of growth is generally controlled by salinity, a function of tidal inundation and therefore elevation. The appearance of the vegetation at Ragged Rock Creek marsh is a mosaic, ranging from patches of monospecific dominants with discrete boundaries, to mixed-species patches with more diffuse transitions (Fig. 2). While our field survey identified 115 plant species at Ragged Rock Creek marsh (see Section 3.2), the vegetation was

dominated by three communities: 1) salt meadow grass (*S. patens*) often mixed with spike rushes (*Eleocharis* species), 2) narrow-leaved cattail (*Typha angustifolia*) and hybrid cattail (*Typha × glauca*) and 3) non-native common reed (*P. australis*). *Typha* spp. and *Phragmites* occupied the mid-to high marsh areas and upper border, typically forming dense monotypic stands. The distribution of *Phragmites* was strongly correlated to the mosquito ditches that exist throughout the marsh, a pattern that has been documented in other studies (e.g., Bart & Hartman, 2000).

3. Data processing and methods

3.1. Spectral data collection and processing

Reflectance spectra were obtained using an ASD Fieldspec FR® spectroradiometer (Analytical Spectral Devices, Boulder, CO) with a wavelength range of 350–2500nm, a sampling interval of 1.4nm between 350–1000nm and 2nm between 1000–2500nm, and a spectral resolution of 3nm between 350–1000nm and 10nm between 1000–2500nm. Individual spectral measurements were an average of 5–10 scans and each canopy was generally sampled 10 or more times. These samples were then averaged to provide a single spectrum for each target for which a standard deviation was calculated. Reflectance spectra were normalized to a white Spectralon® (Labsphere, Inc., North Sutton, NH) panel.

Reflectance spectra were collected for the three dominant vegetation communities at two sites in Ragged Rock Creek marsh (Fig. 2): *S. patens* meadows (*S. patens* ± *Eleocharis* spp., hereafter referred to as *S. patens*), *Typha* spp. (*Typha angustifolia* and/or *Typha × glauca*) and *P. australis*. To document between- and within-plant phenology, field spectra were collected from specific stands of each of the three plant communities monthly in the summer of 2004 at Site 1, approximately biweekly at Site 2 in the summer of 2005 and on a single date in the fall of 2006 (Fig. 2, Table 1). The selected stands were dense monocultures in order to approximate species' endmember characteristics.

The spectrometer is equipped with a 1-meter long fiber optic sensor with a 25° field of view. Spectra were measured by hand-positioning the fiber optic sensor approximately at nadir within 1 meter of the species canopy. Late in the growing season, the height of *Phragmites* prohibited a nadir view and canopy spectra were measured at an oblique angle. The canopy spectra may include background contributions from water, soil, wrack and shade. Understory species were not observed at the target stands. To minimize the effects of shade, spectra were measured between 1000 and 1400h, except for 1 October 2005, where the tides limited marsh access to the late afternoon (approximately 1600h). All spectra were measured at or near low tide when there was no standing water on the marsh. The relative contributions of photosynthetic and non-photosynthetic vegetation to the spectra in these dense monocultures changed throughout the growing season, where background contributions to the FOV of the sensor were visually estimated to be minimal when plant leaves were mature.

To better correlate the field spectra to satellite data, individual field reflectance spectra were averaged over the four QuickBird band intervals (Band 1 (blue): 450–520nm, Band 2 (green): 520–600nm, Band 3 (red): 630–690nm and Band 4 (NIR): 760–900nm (Fig. 3) to

Table 1
Dates of data acquisition at Ragged Rock Creek marsh

Year	May	June	July	Aug	Sept	Oct
2004	14	15	14	19	21	
		27	<u>2</u>	<u>20</u>	<u>12</u>	8
2005		27	27	13	1 12 26	9
		2	<u>17</u>	23		1
2006		← Vegetation survey →				8
				31	<u>13</u>	

Regular font indicates QuickBird image collection, bold font indicates field spectra collection, italics indicate airborne LiDAR data collection. Underlined dates indicate the QuickBird images used in classification.

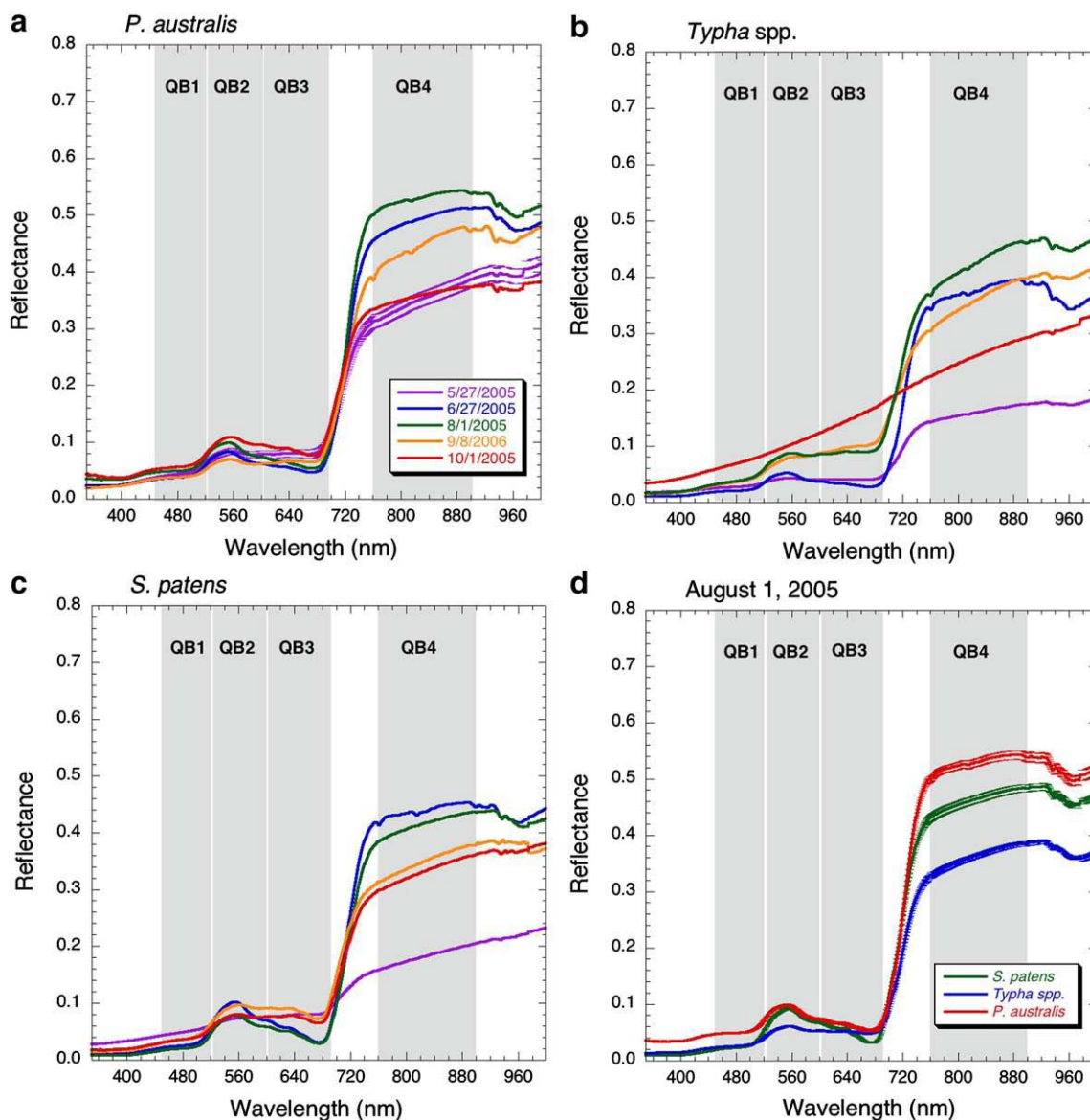


Fig. 3. Example reflectance spectra of major plant species in Ragged Rock Creek marsh. Each spectrum is an average of ≥ 10 spectra. QuickBird band positions are indicated. Collection sites indicated in Fig. 2c. Spectra of (a) *Phragmites*, (b) *Typha* spp., and (c) *S. patens* throughout the growing season. Key in figure (a) corresponds to figures (b) and (c). One standard deviation of the averaged spectra is plotted for *Phragmites* on May 27, 2005 in (a) and is typical of the reflectance data shown in all panels. (d) Spectra of major marsh plant communities on August 1, 2005. One standard deviation of the averaged spectra is plotted.

produce a simulated QuickBird band value. From these data, four spectral indices were calculated and found to be most useful for discrimination of plant species: green/blue, NIR/red, red/green, and the Normalized Difference Vegetation Index ($NDVI = (NIR - red)/(NIR + red)$). The values of these indices over the growing season comprise a set of “radiometry rules” that were used to guide image segmentation and classification. Vegetation indices were used for classification instead of raw bands because they reduce data volume, provide information not available in a single band (Coppin & Bauer, 1996), and normalize differences in reflectance when using multiple images (Singh, 1989) and comparing field and satellite data.

3.2. Collection of the validation set

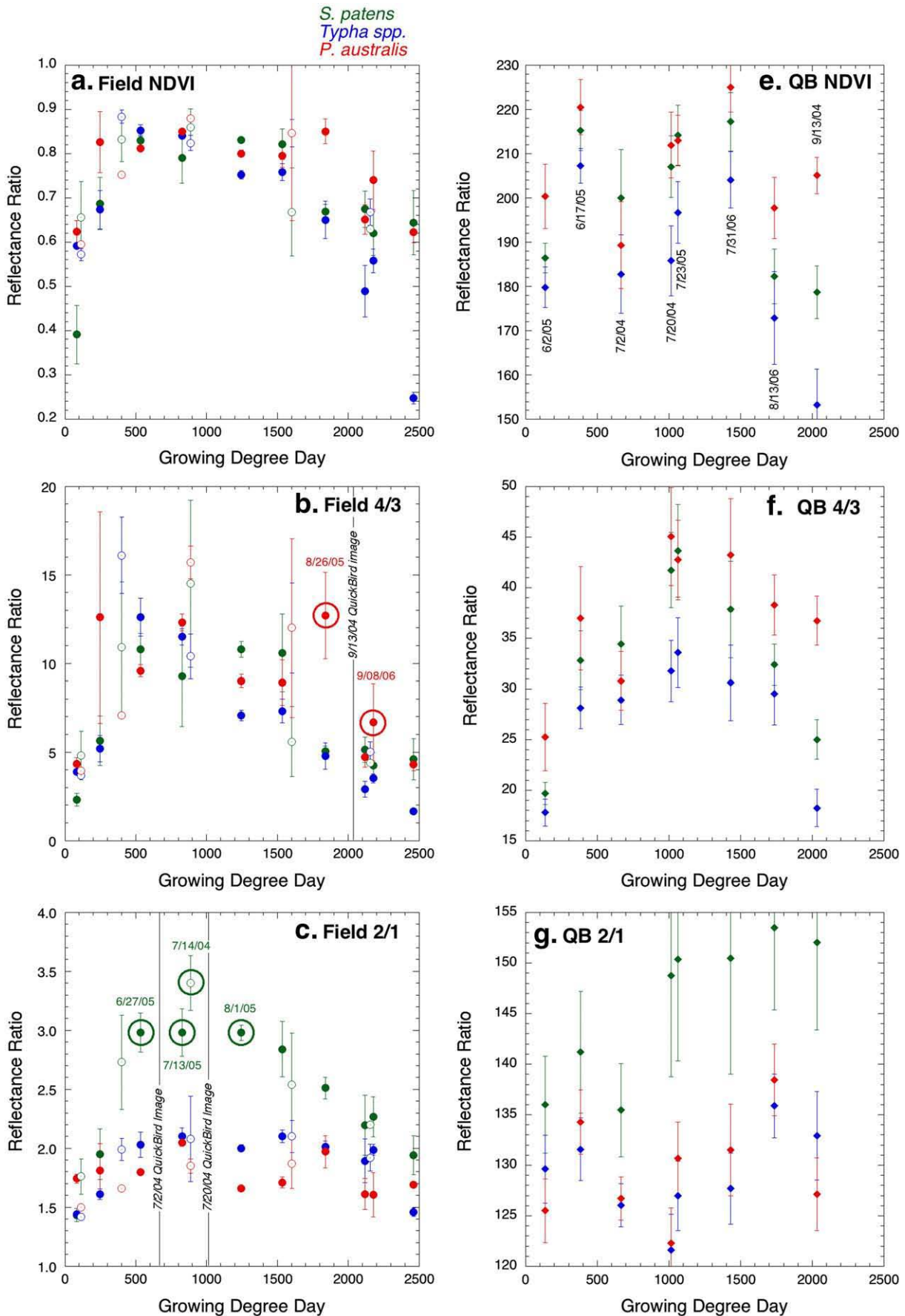
A floristic inventory of the marsh was conducted throughout the summer of 2006 to establish validation data for the image classification. A set of 1000 randomly distributed point locations within the marsh was generated using Hawth's Analysis Tools for ArcGIS (Beyer, 2004). At each location, 4m² quadrats were placed and plant

community composition and species abundance were recorded. GPS field coordinates for the center of each sampling site were recorded and differentially corrected. In total, 923 vegetation plots were

Table 2
QuickBird band ratios used for image segmentation

Image date	Image weights			Raw Bands 1, 2, 3, 4	LiDAR
	Band 2/ Band 1	Band 3/ Band 2	Band 4/ Band 3		
17 June 2005	–	–	0.5	–	–
2 July 2004	0.5	0.5	–	–	–
20 July 2004	0	–	–	Bands 1, 2, 3 = 0.8 Band 4 = 1.0	–
13 August 2006	0.5	0.5	0.5	–	–
12 September 2004	0.5	0.5	0.5	–	–
8 October 2004	–	–	–	–	1.0

The values indicate the weights applied in eCognition™ during image segmentation. The 20 July 2004 2:1 ratio is the only one to not have a weight of 0.5 due to the inclusion of the raw QuickBird bands from this date.



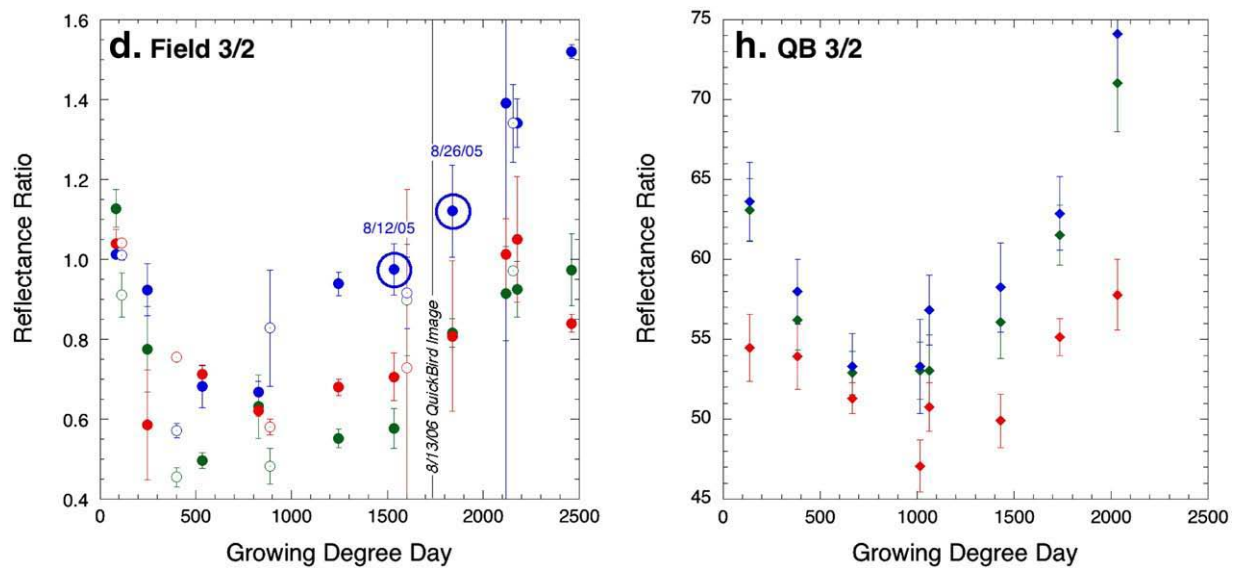


Fig. 4. VNIR reflectance of *Phragmites*, *Typha* spp. and *S. patens* over the 2004–2006 growing season. Average accumulated growing degree days = (average daily temperature – 50°F). Field reflectance data recalculated as QuickBird (QB) bands: (a) NDVI, (b) Bands 4/3, (c) Bands 2/1, (d) Bands 3/2. Each point is an average of ≥ 10 field measurements; error bars are one standard deviation. Dates of spectra acquisition are indicated in Table 1 where open symbols correspond to 2004 and closed symbols to 2005/6. Circled data points refer to dates when spectral differences between the species were utilized to create classification rules for each species in available QuickBird images (indicated). Average reflectance values of image segments in QuickBird data containing the field targets (see Fig. 2c), one standard deviation is plotted: (e) NDVI, (f) Bands 4/3, (g) Bands 2/1, (h) Bands 3/2. Image acquisition dates are indicated in panel (e).

recorded at Ragged Rock Creek; 877 were random plot locations and 46 were locations selected by the field teams as unusual, rare or monotypic plant communities. The spectral reflectance collection sites were included in the 923 plots. Some plots were revisited during the growing season but only one data point was maintained for each plot location resulting in a grand total of 917 field points. For the purposes of accuracy assessment, all points were assigned to one of five dominant classes: *Phragmites*, *Typha* spp., *S. patens*, Water, and Other/mixed to correlate with the classification (Section 3.5).

3.3. Image and LiDAR processing

High-resolution (2.44-meter at nadir) QuickBird satellite image data were acquired for a 100km² area at the mouth of the Connecticut River (Fig. 1) on 9 dates from July 2003 through November 2006 (Table 1). The data were re-projected into the UTM coordinate system, WGS84 datum, zone 18, meters. Each image was co-registered to the 20 July 2004 QuickBird image to assure consistent alignment. Of the nine scenes, five (Table 1, underlined) were selected for the final classification based on image quality (i.e., lack of clouds and haze), acquisition month and day and importance as determined by field spectra data analysis. Although the images spanned several growing seasons, the month and day of acquisition was considered more important than the year of acquisition because the monthly spectral variability was observed to be much greater than interannual variability in the dataset.

Multiple return LiDAR data were collected on 8 October 2004 at an altitude of 3000ft using a Leica ALS50 airborne laser scanner. Two returns per pulse (first and last) were recorded. The LiDAR data points had a nominal ground sampling distance of 0.9m and a reported horizontal accuracy of 0.5m. Based on 22 points, the average error between the bare earth LiDAR coverage and the control was 0.002m with an RMSE of 0.057m. LiDAR non-ground data points for the project area were re-projected to UTM Zone 18N, NAD83, meters and were converted to a 2.4m resolution elevation grid using the Natural Neighbors interpolator in the 3D Analyst Extension to ArcGIS. The elevation grid was converted to an 8-bit unsigned integer format for

use in the eCognition™ software. The elevation grid approximated the top of the plant canopy within the study area.

3.4. Classification

Classification was conducted using the hierarchical object-oriented image analysis software eCognition™ (Benz et al., 2004). Input data (layers) consisted of QuickBird images comprised of single bands from a single date, band ratio images on multiple dates (Table 2), and LiDAR top of canopy information. Non-marsh features such as houses, trees and lawns were eliminated from the input data. The input data were segmented into image objects, which are contiguous pixels that are grouped together into homogeneous polygon features. The advantage of an object-oriented approach is that both spectral and spatial parameters define an image object; this is in contrast to per-pixel classifiers where each pixel is treated independently of all others, including its neighbors. In this study, spectral and spatial parameters (smoothness and compactness) were set to contribute 70% and 30%, respectively, to the segment boundary definition. Each layer in the eCognition™ project was weighted to determine its contribution to the segmentation (Table 2). The relative size of each image object is determined by a scale parameter, which sets the maximum allowed heterogeneity between image objects. A scale parameter of 20 was found to be the optimum size that best corresponded to the plant communities within the Ragged Rock Creek marsh using QuickBird data. The result is a segmented image consisting of objects, each of which is treated as a single entity in the classification.

3.5. Accuracy assessment

Two-thirds of the field points from the floristic inventory ($n = 613$) were used for accuracy assessment, but only those that were at a distance greater than 2m ($n = 379$) from each class boundary were used to ensure that the points were located within the class being evaluated and that GPS inaccuracies and image registration errors were not factors. The accuracy assessment used the fuzzy set approach of Gopal and Woodcock (1994) which acknowledges the inherent

variation in vegetation communities by allowing for sites to exhibit some grade of membership among map classes. For example, sites may reasonably be members of multiple classes, or alternately, some sites may only show a poor resemblance to any of the map classes.

The Gopal and Woodcock (1994) fuzzy accuracy assessment method uses a rating system of linguistic levels of increasing correctness, labeled: (1) *Absolutely Wrong*, (2) *Understandable but Wrong*, (3) *Reasonable or Acceptable Answer*, (4) *Good Answer*, and (5) *Absolutely Correct*. Each field point in the validation set was assigned a linguistic value between 1 and 5 corresponding to membership in one of four classes: *Phragmites*, *Typha* spp., *S. patens*, and Other/mixed. Ratings were initially assigned based on a statistical method where the Euclidean distances in ordination space to class centroids (Podani, 2000, ter Braak and Šmilauer, 1998) were inversely translated into ordinal ranks that related to the five linguistic levels. Additionally, "expert" judgment was made, without knowledge of the map labels, to make adjustments in linguistic fuzzy values for the conspicuous dominance or absence of major species. The accuracy assessment was completed by comparing the vegetation class rating of each validation site to the QuickBird classification result.

4. Results

4.1. Phenology and structure of major species

The canopy reflectance spectra of each plant community were broadly similar, including absorptions typical of healthy photosynthesizing vascular plants (Fig. 3). At the beginning of the growing season, each spectrum showed expected increases in the strength of the absorptions at approximately 450nm and 680nm due to chlorophylls and carotenoids within the leaves and an increase in NIR reflectance due to leaf biomass (e.g., Wooley, 1971). This trend continued in each species until the onset of senescence (Fig. 3a–c). Comparison of the spectra of individual species showed that the magnitude and shape of the spectra can differ qualitatively on individual dates (Fig. 3d).

To relate the spectral variability of the field data to QuickBird images, the reflectance spectra of each species were reduced to simulated QuickBird band ratios and plotted as a function of average accumulated growing degree days (GDD_{50} = (average daily temperature - 50°F (10°C))) using temperature data records for the Groton, Connecticut airport acquired by the National Climatic Data Center (Fig. 4). Trends of NDVI and the NIR/red ratios were similar to each other, where the NIR/red ratio provided greater separability amongst the individual points (Fig. 4a,b). All species showed a rise in these indices at approximately GDD_{50} 400 (early June) corresponding with the green-up phase of plant growth and a subsequent decline in the indices corresponding to senescence. *S. patens* and *Phragmites* reached peak values at ~ GDD_{50} ≥ 900 (mid-July) and *Typha* spp. at ~ GDD_{50} 500 (mid- to late June). *Typha* spp. NDVI and NIR/red values were generally higher than the other species near the time of their peak while *Phragmites* values exceeded the other species in mid-August through early September.

The seasonal pattern of the simulated QuickBird green/blue ratio of *S. patens* was unique (Fig. 4c). Values of this ratio were similar for each species at the beginning of the season, but *S. patens* rose to a peak value near GDD_{50} 900 (mid-July). The absolute value of this ratio for *S. patens* was twice that of *Typha* spp. and *Phragmites* from early June through early August.

The general seasonal pattern of the simulated QuickBird red/green ratio for all species showed an initial decline from approximately GDD_{50} 200 to GDD_{50} 800 (late May–late June) and then an increase (Fig. 4d). *S. patens* values in this index were lower than the other two species over GDD_{50} 400 to 1500 (mid-June–early August). *Typha* spp. values exceeded those of the other species from mid-July onward.

Three simple band ratios were determined to be most useful in identifying at least one major plant community: for *Phragmites*, the

NIR/red ratio in late summer, for *S. patens*, the green/blue ratio in midsummer, and for *Typha* spp., the red/green ratio in late summer (circled points, Fig. 4). These periods showed both the greatest spectral separability between individual species and the best correspondence with the dates (month, day) of the QuickBird images available for classification (Table 1; Fig. 4).

On the Ragged Rock Creek marsh, the average height of *Phragmites* determined from the field survey points was 2.1m ($n = 213$), *Typha* spp. points averaged 1.1m ($n = 206$) and *S. patens* points averaged 0.7m ($n = 160$; Fig. 5). The LiDAR data generally agreed with field observations of each species' growth habit in October.

4.2. QuickBird classification

Fig. 6 graphically illustrates the rules that were identified from the field spectra and implemented in the classification of the QuickBird images. QuickBird classification results are displayed in Fig. 7. Qualitatively, the classification identified contiguous areas of *Phragmites*, *Typha* spp., and *S. patens*. The classification confirmed that the portion of Ragged Rock Creek marsh surveyed was dominated by the three species under study, where classified *Typha* spp. and *Phragmites*, comprised 36% (45.2 ha) and 24% (30.5 ha) respectively, *S. patens* covered 22% (27.8ha), and other species covered 18% (22.9ha) of the marsh.

The frequency of correct matches (and mismatches) for each map class and the overall (total) map were calculated by using two fuzzy accuracy measures, MAX and RIGHT (Table 3; all fuzzy measures are derived from Gopal and Woodcock (1994)). The MAX column indicates the strictest measure of accuracy where only the highest membership level (5) was acceptable; this is the closest measure to traditional accuracy assessment (Congalton & Green, 1999). The RIGHT column indicates an acceptable map label choice (a linguistic level of ≥ 3). *Phragmites* had the highest accuracy with both MAX and RIGHT values of 97%. *Typha* spp. was the least accurate with 63% MAX and 76% RIGHT. The *S. patens* meadows type was labeled correctly in most cases with a MAX of 80% and RIGHT of 92%. The category Other/Mix had a MAX value of 72% but a RIGHT value of 100%. In general, the total weighted accuracy of all map labels adjusted for areal proportion of each map class had a MAX rating of nearly 77% and an acceptable RIGHT rating of nearly 89%.

The magnitude of errors measures the difference scored between the map assigned linguistic level and the highest linguistic level given in the field data (Table 4). A measure of 4 is the "perfect" case where the mapped category is perfectly right (5) and all other categories are perfectly wrong (1). An error difference of - 1 occurs when the map label level is only one level away from the highest level of the field data; errors may increase to a - 4. The arithmetic mean of these values is interpreted as a summary measure inversely proportional to error severity, hence larger mean values are indicative of a higher overall quality of the map. *Phragmites* was the most reliably-mapped class where 47 of the 68 points (69%) had perfectly correct assignments and a high arithmetic mean of 2.97. *S. patens* had the second highest

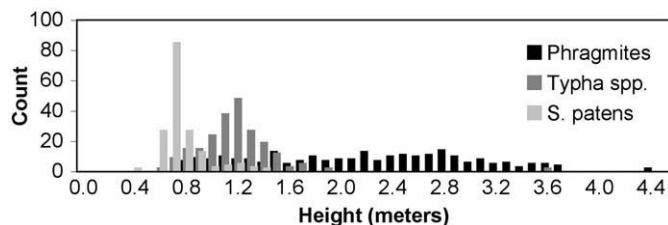


Fig. 5. Histograms showing LiDAR height data for GPS field inventory plots where each plant class is dominant.

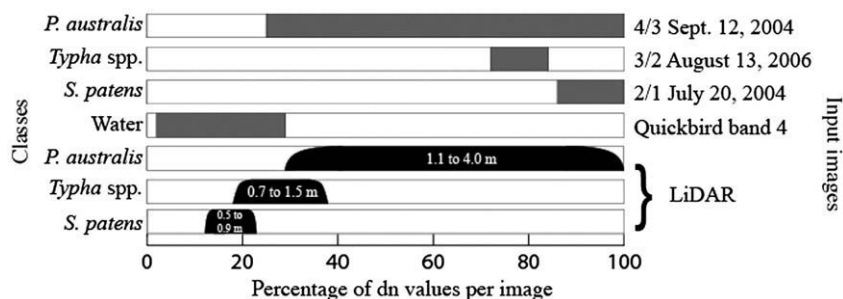


Fig. 6. Knowledge-based rules (in grey and black) implemented in eCognition™ for the classification of image objects. Each bar corresponds to one rule that was applied to an image (right hand side) used to define each class (left hand side). The percentage (x axis) was calculated based on the maximum digital number (dn) for each image. For example, *Phragmites* image objects were defined by having high values of the NIR/red ratio in the 12 September 2004 QuickBird image (~ uppermost 75% of dn values in the image) and high values (1.1 to 4.0 m) in the LiDAR data. High values of the red/green band ratio in the 13 August 2006 QuickBird image and middle heights of LiDAR identified *Typha* spp. objects. High values of the green/blue band ratio in the 20 July 2004 QuickBird image and low values of the LiDAR height data determined *S. patens* objects. Water was identified by low Band 4 values in the 20 July 2004 QuickBird image.

arithmetic mean of 1.71. *Typha* spp. had a low arithmetic mean (0.77). *Typha* spp. had the greatest spread of errors, including 19% of the total in the - 4 category. The Other/Mix class had the lowest arithmetic mean of 0.43 due primarily to the large numbers of equivalent class assignments (as indicated by the proportion of values in the middle range from - 1 to 1) and not due to errors of large magnitude.

Sources of error resulting from sites with multiple memberships are presented in Table 5. *Phragmites* was the most correctly mapped class, with a high frequency of single membership sites (49 of 68 points, 72%) that were correctly matched (100%). Just over half of the *Typha* spp. points (85 points, 54%) had a single membership and of these, most points were correctly matched. *Typha* spp. was the only

case where there were more mismatches than matches in the classes with multiple memberships eroding the confidence of that map label. By the very definition of fuzzy sets, correct maps will have classes with many multiple memberships, especially as was the case with the Other/Mix class and the *S. patens* meadow. Just over half of the *S. patens* points (47 points, 52%) had a single membership, and of these almost 90% were classified correctly; 60% of the multiple membership points were classified correctly. The majority of points in the Other/Mix class had multiple memberships.

The categorical nature of errors i.e., pairwise error within and between categories are summarized in Fuzzy Confusion and Fuzzy Ambiguity matrices (Tables 6 and 7). The Fuzzy Confusion function,

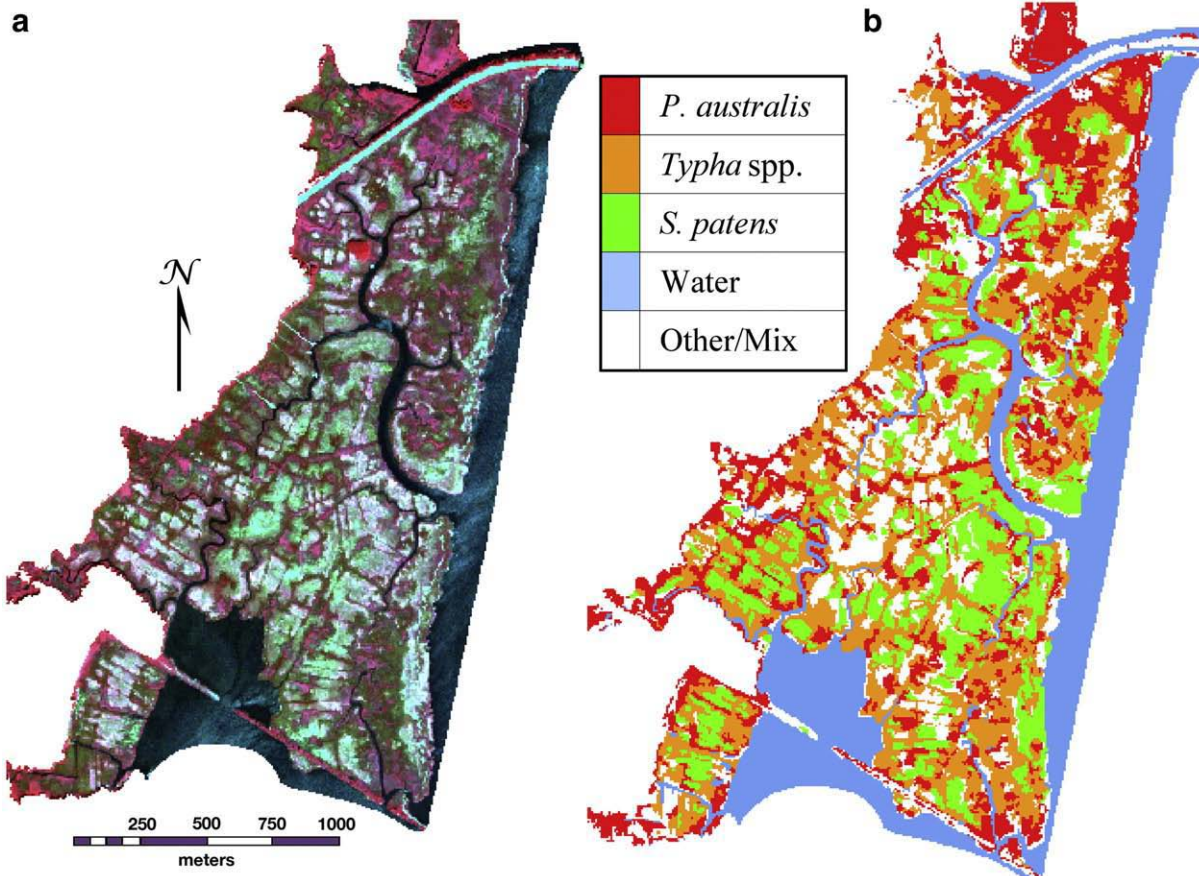


Fig. 7. (a) 20 July 2004 QuickBird 4-2-1 image. (b) Classification result.

Table 3
Frequency of correct matches for all map label categories based on two fuzzy operator choices: best choice, MAX (M) where linguistic level=5 and acceptable choice RIGHT (R), with a linguistic level ≥3

Map label	Sites	Technical evaluation of matches (ground data)				Area weights
		MAX (M)		RIGHT (R)		
		Improvement (R-M)				
<i>Phragmites</i>	68	66 (97.1%)	66 (97.1%)	0	(0.0%)	0.24130
<i>Typha</i>	157	99 (63.1%)	119 (75.8%)	20	(12.7%)	0.35783
<i>S. patens</i>	90	72 (80.0%)	83 (92.2%)	11	(12.2%)	0.21994
Other/Mix	64	46 (71.9%)	64 (100.0%)	18	(28.1%)	0.18093
Total	379	283 (74.7%)	332 (87.6%)	49	(12.4%)	1
Weighted total		(76.5%)	(88.8%)		(12.3%)	

The overall accuracy of all map labels, i.e., the entire map, is given as the total. Area weights were determined by the contributing areal proportion of the map label categories.

Table 4
Fuzzy difference matrix

Map label	Sites	Mismatched (ω_c)					Matches (ϖ_c)				Arithmetic mean
		-4	-3	-2	-1	0	1	2	3	4	
		<i>Phragmites</i>	68	2	0	0	0	7	3	8	
<i>Typha</i>	157	29	7	14	8	11	5	14	15	54	0.77
<i>S. patens</i>	90	3	4	5	6	12	7	11	3	39	1.71
Other/Mix	64	0	0	0	18	14	23	3	6	0	0.45
Total	379	34	11	19	32	44	38	36	25	140	1.34

The magnitude and severity of errors in the fuzzy assessment resulting from the difference in linguistic membership value between the map label score and the highest score assigned to all classes of the field data. Correctly mapped areas have zero and positive values, where well-mapped areas have high positive scores. Negative values coincide with map errors and large errors result in high negative scores. The arithmetic mean summarizes the severity of the error and, hence, it is indicative of map quality.

Table 5
Sources of error for map classes as a function of multiple memberships attaining an acceptable level (linguistic level equal to 3 or better) at each site

Map label	Sites	Membership (χ)											
		1			2			3			4		
		T	M	N	T	M	N	T	M	N	T	M	N
<i>Phragmites</i>	68	49	49	0	12	11	1	7	7	0	0	0	0
<i>Typha</i>	157	85	69	16	48	21	27	18	7	11	6	2	4
<i>S. patens</i>	90	47	42	5	36	25	11	6	4	2	1	1	0
Other/Mix	64	9	9	0	37	24	13	17	12	5	1	1	0
Total	379	190	169	21	133	81	52	48	30	18	8	4	4

Total numbers of sites (T) are further subdivided into correctly matched (M) and mismatched sites (N). See text for discussion.

Table 6
Fuzzy Confusion Matrix

Map label	Sites	Technical evaluation (ground data)					Commission errors
		<i>Phragmites</i>	<i>Typha</i>	<i>S. patens</i>	Other/Mix	No. of mismatches	
		ζ_{cc}	ζ_{cc}	ζ_{cc}	ζ_{cc}	ζ_{cc}	
<i>Phragmites</i>	68	X	0	1	2	3	4%
<i>Typha</i>	157	29	X	30	42	101	64%
<i>S. patens</i>	90	2	2	X	17	21	33%
Other/Mix	64	3	6	9	X	18	28%
Total	379	34	8	40	61	143	
Omission errors		34%	5%	31%	49%		

The Confusion function, ζ_{cc} , identifies samples where the map label was not the highest rating resulting in a mismatch. The category with the highest rating is shown by the technical evaluation assignment.

Table 7
Fuzzy Ambiguity Matrix

Map label	Sites	Technical evaluation (ground data)				No. of mismatches
		<i>Phragmites</i>	<i>Typha</i>	<i>S. patens</i>	Other/Mix	
		η_{cc}	η_{cc}	η_{cc}	η_{cc}	
<i>Phragmites</i>	68	X	4	0	7	11
<i>Typha</i>	157	2	X	5	11	18
<i>S. patens</i>	90	2	0	X	12	14
Other/Mix	64	4	5	8	X	17
Total	379	8	9	13	30	60

The Ambiguity function, η_{cc} , identifies cases where the mapped category had the same rating as another category. It was only applied to acceptable ratings (score of 3 or better). See text for discussion.

ζ_{cc} , (Table 6) identifies mismatched sites, and is nearly equivalent to a conventional confusion matrix of Congalton and Green (1999). The map label column in the table identifies which map category was assigned. *Phragmites* had the lowest number of commission errors. *Typha* spp. has the highest number of commission errors and the lowest number of omission errors, as *Typha* spp. comprised correctly and incorrectly many of the mapped categories in the classification.

The Fuzzy Ambiguity function, η_{cc} , (Table 7) identifies categories with the same rating as the mapped category only when the ratings were acceptable (linguistic level 3 or better). The off-diagonal values are mismatched, but retain some degree of correctness. The Other/Mix class was the most ambiguous, a testimony to its transitional nature. The Other/Mix column contained a total of 30 sites that were considered equivalent to the mapped category. Furthermore, Other/Mix was also mapped as an equivalent in 17 sites categorized by ground truth as something else. *Phragmites* was the least ambiguous. It contained 4 sites equally rated with *Typha* spp. *Typha* spp. also included 5 sites that had an equivalent rating with *S. patens* and 2 sites with *Phragmites*. *S. patens* had 0 points with equivalent rating of *Typha* spp. The asymmetry in the matrix revealed that ambiguous points between *Typha* spp. and *S. patens* would most likely be mapped as *Typha* spp.

5. Discussion

5.1. Spectral characteristics of marsh species across the growing season

The spectral characteristics of vegetation are due to leaf pigments, plant structure (e.g., biomass and canopy architecture and cover) and plant health throughout the phenological cycle. Much of the spectral variability in the field data can be attributed to expected increases in plant pigments and biomass during the green-up phase of plant growth, and the decline of these variables and the increased contribution of background materials during senescence. The magnitude and rate of these changes is found to differ in individual species allowing their spectral discrimination at specific times during the growing season. The variability observed in individual reflectance spectra measured in the field was replicated when these spectra were resampled to QuickBird bands. Simple spectral indices were sufficient to distinguish the three dominant plant communities within a mosaic of other vegetation in Ragged Rock Creek marsh.

Many studies have shown a correlation between the near-infrared reflectance of vegetation and biomass in general and in marsh species in particular (e.g., Drake, 1976; Hardisky et al., 1984, Hardisky et al., 1986; Gross et al., 1993; Zhang et al., 1997). We suggest this correlation is apparent in the field data where *Phragmites* and *Typha* spp., which often occur as monocultures, had higher NDVI and NIR/red values throughout the growing season than the low-growing *S. patens* (Figs. 4a, b, e). NIR index values peaked for *Typha* spp. in mid-late June, corresponding to field observations of peak plant heights, full development of flowers and wholly green leaves. *Phragmites* displayed

peak NIR index values in mid-August to early September correlating to peak plant heights and the development of flowers. Moreover, by late August, *Typha* spp. had senesced resulting in a reduction in green biomass and likely an increase in the contribution of background materials such as wrack or soil to its spectrum. These factors should reduce NIR and increase the red values for *Typha* spp. relative to *Phragmites* (e.g., Hardisky et al., 1984).

The green/blue ratio of *S. patens* was dramatically higher than that of *Phragmites* or *Typha* spp. from mid-June through late August (Fig. 4c). We attribute this to inherent differences in the amount of chlorophyll *b* and carotenoids in these species, both of which absorb in the blue portion of the spectrum (Fig. 3). The peak in the green/blue index for *S. patens* in mid-July corresponds to maximum pigment concentration at this time of year.

Our field data generated the following set of spectral rules that may be applicable to the discrimination of *Phragmites*, *Typha* spp. and *S. patens* communities: 1) *Phragmites* is best distinguished by its high NIR response late in the growing season, 2) *Typha* spp. is best distinguished by high red/green response in August, and 3) *S. patens* is best distinguished by a unique green/blue ratio throughout the growing season. Our field data predict that seasonal spectral behavior should be evident within actual QuickBird data. To demonstrate this, we identified the image segments on 8 QuickBird images that contained the sites where the field point spectra were measured in 2005 and 2006. Average band ratios for all pixels within each segment were plotted in Fig. 4e–h. In the QuickBird data, *Phragmites* uniquely displayed high NDVI and NIR/red values late in the growing season (Fig. 4e,f), and *S. patens* had a relatively high green/blue values throughout the growing season (Fig. 4g). The red/green values for *Typha* (Fig. 4d) are greater than and separable from *Phragmites* throughout the growing season, but overlapped with *S. patens*. Thus simple indices in 4 band data such as QuickBird were adequate to remotely measure and distinguish the spectral characteristics of these species over the growing season.

The values of the QuickBird data spectral ratios for the field targets over the growing season follow the patterns established in the field data. This supports the use of field spectra for the training of image classifiers as has been predicted by other studies (e.g., Silvestri et al., 2002; Wang et al., 2007). As the QuickBird data were collected at various times of day and tidal height, the correspondence between field and satellite data suggests that the canopy spectra at the satellite level was dominated by vegetation and the contribution of variable background elements like water and shade was minimal. The field targets were selected because they are monocultures with high areal density, so we expected little to no contribution of understory species in these data. Understory species may become an important part of the canopy spectrum in less dense stands, which may reduce classification accuracy (see Section 5.2).

The phenological trends seen here can vary as a function of plant vigor, which may depend on changes in salinity, climate, predation or disturbance. Corrections for interannual and regional changes in these factors must therefore be performed when attempting to interpret classification results or select dates to maximize interspecies spectral discrimination. However, the spectral trends noted here may have broader spatial and temporal application. We emphasize that in this study, the phenological behavior of the spectral indices is consistent over 3 years at two separate areas in both the field and satellite data of Ragged Rock Creek marsh. Furthermore, other studies show similar spectral behavior of wetland plant species. The late season peak in NIR reflectance we observed in our data for *Phragmites* is also noted for this species in VNIR field spectra measured in the New Jersey Meadowlands (Artigas & Yang, 2005, 2006) and in the Yangtze Estuary (Gao & Zhang, 2006). *Phragmites* is also found to be most spectrally separable from *Typha* spp. in field VNIR spectra measured in the Hudson River estuary in late August (Laba et al., 2005). These studies suggest that the spectral variability utilized here may be

applied to other areas, particularly if guided by any ecological assessment of growth habits of marsh species locally.

5.2. Classification

The fuzzy accuracy assessment utilized two measures of accuracy for each class: MAX (best) and RIGHT (correct). The highest MAX accuracies were reported for validation points containing a single species. Our classification approach was the most useful for discriminating *Phragmites*, which occurred most often as monotypic stands. Yet, the marsh mosaic also included another, and perhaps more typical scenario, where several species are admixed in varying amounts. Treating the validation points in this study with linguistic values, fuzzy accuracy assessment and the RIGHT accuracy measure enabled an arguably more realistic interpretation of vegetation stands with co-dominant or transitional species typical of many marshes and returned a higher accuracy than the MAX measure. Similar improvements in accuracy between MAX and RIGHT measures have been noted for the mapping of marsh vegetation using QuickBird imagery (Laba et al., 2008) with eCognition™ (Yu et al., 2006).

Examination of points misclassified as *S. patens* included bare ground/flotsam/wrack, which are all low-lying and spectrally bright and other low-growing species such as blackgrass (*Juncus gerardii*), bentgrass (*Agrostis stolonifera*) and switchgrass (*Panicum virgatum*). Using the RIGHT accuracy measure improved results for *S. patens*, which we suggest resulted from its distribution as understory in many of the validation quadrats. In these situations, the spectral signature of *S. patens* contributed to the signal even if fewer disperse, taller species dominate the LiDAR first return (canopy) data.

Typha spp., the most overmapped class, was confused with *Phragmites* and a number of species. Examination of the validation data shows that the classification misidentified many points where *Typha* spp. was recorded in low abundance (Fig. 8). These points contain *Typha* spp., which occasionally has a diffuse clonal growth habit, within a mix of species of various heights, spectral signatures and densities. Many of these species, like *Phragmites*, are observed to occur at similar heights (approximately 1–2m) to *Typha* spp. during the middle part of the growing season, including sedges (*Schenoplectus* species) and bulrushes (*Bolboschoenus* species). The wide range of species that are confused with *Typha* spp. is likely exacerbated by its lack of an extreme, defining spectral or height rule (Fig. 5). In contrast, both *Phragmites* and *S. patens* have extremes in the LiDAR data (tallest

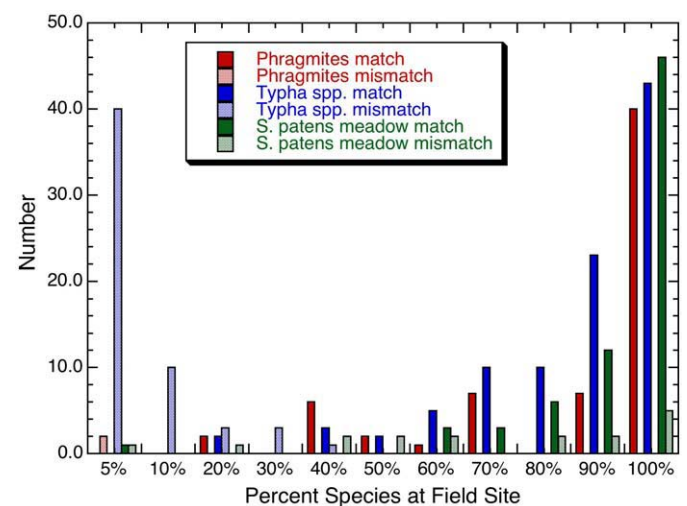


Fig. 8. Vegetation community abundance determined by field observation compared the best choice (fuzzy operator MAX, Table 3) map classification label. Correctly mapped species have a high number of matches.

and shortest, respectively) and have one band ratio that is quite distinct (late season NIR/red and mid-season green/blue, respectively). The fact that *Typha* spp. covers the largest area of the marsh may also increase the potential for confusion and error.

Elevation information, such as that derived from LiDAR, is an important feature of natural vegetation classification (Morris et al., 2005; Rosso et al., 2006; Sadro et al., 2007; Yu et al., 2006). *Phragmites* was observed to be approximately 1m taller than the next tallest species in late summer. This characteristic distinguishes *Phragmites* from *Typha* spp. and *S. patens* in the LiDAR data (Fig. 5), likely contributing to the success of its classification. While it is possible that the use of LiDAR as a sole discriminant could identify a large proportion of *Phragmites* occurrences, the spectral characteristics are likely necessary to distinguish between *Phragmites* and *Typha* spp. because there is considerable overlap in the height data of these species.

The accuracy of the classification methodology reported here is comparable to that of a variety of supervised classifiers used to map tidal marsh vegetation in QuickBird (Belluco et al., 2006; Laba et al., 2008) and CASI images (Wang et al., 2007).

5.3. Implications for mapping of salt marsh vegetation

The canopy spectral and structural characteristics of *Phragmites*, *Typha* spp. and *S. patens* vary as a function of plant phenology in both field collected spectra and QuickBird images (Fig. 4). The plant communities were found to be spectrally separable in 4 band data and thus we predict that other four-band image systems could be used for marsh plant classification, obviating the need for hyperspectral airborne data (e.g., AVIRIS or CASI). The high spatial resolution of QuickBird images likely contributed to the success of the classification; we would expect classification accuracy to degrade with lower spatial resolution data (e.g., Landsat) as has been noted in other attempts to classify salt marsh vegetation (Belluco et al., 2006).

The seasonal variations in spectral behavior make clear the necessity of multi-temporal imagery for mapping multiple species on a complex tidal marsh. Our study demonstrates that field observations at a limited number of reference sites were sufficient for classification. The spectral and structural data predicted times during the growing season when each species was best discriminated. With this knowledge, a single date of imagery could be used to adequately map a single species. For example, in Ragged Rock Creek marsh, the high NIR response and height of *Phragmites* in the autumn distinguishes it uniquely among a mosaic of plant species typical of a brackish marsh. Natural resource land managers seeking to monitor *Phragmites* in this region could utilize single date color infrared images (satellite or aerial) and/or LiDAR during late August to early September for *Phragmites* identification. Classification could be accomplished at other marshes with field observations at a limited number of reference sites.

6. Conclusion

This study presents a new technique for the classification of major marsh plant species within a complex, heterogeneous tidal marsh using multi-temporal QuickBird images, field reflectance spectra and LiDAR height information. Analyses of the phenological variation of spectral and structural characteristics of marsh species measured in the field throughout the growing season were necessary to select the best dates to discriminate *Phragmites*, *Typha* spp. and *S. patens*. These three species are spectrally distinguishable at particular times of year. These distinctions are recognizable both in high-resolution field spectra, in the spectra when degraded to spectral resolution typical of 4 band multispectral sensors, and in QuickBird images of the field sites.

Rules based on the spectral variability of species throughout the growing season were used to direct the classification of multi-temporal QuickBird images. Mapping accuracies were best measured for all species by using a fuzzy accuracy assessment, which

accommodates the complex mosaic of dominant and mixed plant communities of Ragged Rock Creek marsh. Classification accuracies for *Phragmites* were high due to the high NIR reflectance and height of this dense monoculture in the early fall. For classification, the spectral data supplements the LiDAR data as it may include contributions from understory species like *S. patens*.

The results of this study demonstrate the utility of remote sensing to map certain types of marsh vegetation. Although multi-temporal image data were utilized for the classification in this study, the phenological variations recognized here can be utilized for judicious selection and analysis of single date, four-band satellite or aerial image data of coastal marshes along Long Island Sound. Such data are likely to be useful to coastal managers and may greatly facilitate the identification and inventory of marsh species.

Acknowledgements

This study was funded by the EPA Long Island Sound Research Program, grant L197100901. A portion of the data was provided by the NOAA Coastal Services Center Coastal Remote Sensing Project and the Institute for the Application of Geospatial Technology. The 2006 field work was funded by the CT DEP Long Island Sound License Plate Program. We very much appreciate the contributions of Bill Moorhead and Joel Labella in the field and the careful reviews provided by the referees and the editors of this special issue.

References

- Artigas, F. J., & Yang, J. S. (2005). Hyperspectral remote sensing of marsh species and plant vigour gradient in the New Jersey Meadowlands. *International Journal of Remote Sensing*, 26, 5209–5220.
- Artigas, F. J., & Yang, J. S. (2006). Spectral discrimination of marsh vegetation types in the New Jersey Meadowlands, USA. *Wetlands*, 26, 271–277.
- Arzandeh, S., & Wang, J. (2003). Monitoring the change of *Phragmites* distribution using satellite data. *Canadian Journal of Remote Sensing*, 29, 24–35.
- Barrett, N., & Prisloe, S. (1998). Spatial patterns of expansion by *Phragmites australis* (Cav.) Trin. ex Steud. within the tidelands of the Connecticut River from 1968 to 1994. *CD-ROM and report to The Nature Conservancy Middletown, CT*, 1 June 1998.
- Bart, D., & Hartman, J. M. (2000). Environmental determinants of *Phragmites australis* expansion in a New Jersey salt marsh: An experimental approach. *OIKOS*, 89, 59–69.
- Bart, D., Burdick, D., Chambers, R., & Hartman, J. M. (2006). Human facilitation of *Phragmites australis* invasions in tidal marshes: A review and synthesis. *Wetlands Ecology and Management*, 14, 53–65.
- Belluco, E., Camuffo, M., Ferrari, S., Modenese, L., Silvestri, S., Marani, A., & Marani, M. (2006). Mapping salt-marsh vegetation by multispectral and hyperspectral remote sensing. *Remote Sensing of Environment*, 105, 54–67.
- Benz, U. C., Hofmann, P., Willhauck, G., Lingenfelder, I., & Heynen, M. (2004). Multi-resolution, object-oriented fuzzy analysis of remote sensing data for GIS-ready information. *Photogrammetry and Remote Sensing*, 58, 239–258.
- Bertness, M. D., Ewanchuk, P. J., & Silliman, B. R. (2002). Anthropogenic modification of New England salt marsh landscapes. *Proceedings of the National Academy of Sciences*, 99, 1395–1398.
- Beyer, H.L. (2004). Hawth's Analysis Tools for ArcGIS. <http://www.spatial ecology.com/htools>
- Chambers, R. M., Meyerson, L. A., & Saltonstall, K. (1999). Expansion of *Phragmites australis* into tidal wetlands of North America. *Aquatic Botany*, 64, 261–273.
- Congalton, R. G., & Green, K. (1999). *Assessing the Accuracy of Remotely Sensed Data: Principles and Practices*. Boca Raton, FL: Lewis Publishers.
- Coppin, P. R., & Bauer, M. E. (1996). Digital change detection in forest ecosystems with remote sensing imagery. *Remote Sensing Reviews*, 13, 207–234.
- Dennison, P. E., & Roberts, D. A. (2003). The effects of vegetation phenology on endmember selection and species mapping in southern California chaparral. *Remote Sensing of Environment*, 87, 295–309.
- Donnelly, J. P., & Bertness, M. D. (2001). Rapid shoreward encroachment of salt marsh cordgrass in response to accelerated sea-level rise. *Proceedings of the National Academy of Sciences*, 98, 14218–14223.
- Donoghue, D. N. M., & Shennan, I. (1987). A preliminary assessment of Landsat TM imagery for mapping vegetation and sediment distribution in the Wash estuary. *International Journal of Remote Sensing*, 8, 1101–1108.
- Drake, B. G. (1976). Seasonal changes in reflectance and standing crop biomass in three salt marsh communities. *Plant Physiology*, 58, 696–699.
- Farnsworth, E. J., & Meyerson, L. A. (1999). Species composition and inter-annual dynamics of a freshwater tidal plant community following removal of the invasive grass *Phragmites australis*. *Biological Invasions*, 1, 115–127.
- Gao, Z. G., & Zhang, L. Q. (2006). Multi-seasonal spectral characteristics analysis of coastal salt marsh vegetation in Shanghai, China. *Estuarine, Coastal and Shelf Science*, 69, 217–224.
- Gopal, S., & Woodcock, C. (1994). Theory and methods for accuracy assessment of thematic maps using fuzzy sets. *Photogrammetric Engineering & Remote Sensing*, 60, 181–188.

- Gross, M. F., & Klemas, C. (1986). The use of Airborne Imaging Spectrometer (AIS) data to differentiate marsh vegetation. *Remote Sensing of Environment*, 19, 97–103.
- Gross, M. F., Hardisky, M. A., Wolf, P. L., & Klemas, V. (1993). Relationship among *Typha* biomass, pore water methane, and reflectance in a Delaware (U.S.A.) brackish marsh. *Journal of Coastal Research*, 9, 339–355.
- Hardisky, M. A., Daiber, F. C., Roman, C. T., & Klemas, V. (1984). Remote sensing of biomass and annual net primary productivity of a salt marsh. *Remote Sensing of Environment*, 16, 91–106.
- Hardisky, M. A., Gross, M. F., & Klemas, V. (1986). Remote sensing of coastal wetlands. *Bioscience*, 36, 453–460.
- Judd, C., Stenberg, S., Shaughnessy, F., & Crawford, G. (2007). Mapping salt marsh vegetation using aerial hyperspectral imagery and linear unmixing in Humboldt Bay, California. *Wetlands*, 27, 1144–1152.
- Key, T., Warner, T. A., McGraw, J. B., & Fajvan, M. A. (2001). A comparison of multispectral and multitemporal information in high spatial resolution imagery for classification of individual tree species in a temperate hardwood forest. *Remote Sensing of Environment*, 75, 100–112.
- Laba, M., Tsai, F., Ogurcak, D., Smith, S., & Richmond, M. E. (2005). Field determination of optimal dates for the discrimination of invasive wetland plant species using derivative spectral analysis. *Photogrammetric Engineering and Remote Sensing*, 71, 603–611.
- Laba, M., Downs, R., Smith, S., Welsh, S., Neider, C., White, J., Richmond, M., Philpot, W., & Baveye, P. (2008). Mapping invasive wetland plants in the Hudson River National Estuarine Research Reserve using QuickBird satellite imagery. *Remote Sensing of Environment*, 112, 286–300.
- Maheu-Giroux, M., & de Blois, S. (2005). Mapping the invasive species *Phragmites australis* in linear wetland corridors. *Aquatic Botany*, 83, 310–320.
- Meyerson, L., Saltonstall, K., Windham, L., Kiviat, E., & Findlay, S. (2000). A comparison of *Phragmites australis* in freshwater and brackish marsh environments in North America. *Wetlands Ecology and Management*, 8, 89–103.
- Moore, H. H., Niering, W. A., Marsicano, L. J., & Dowdell, M. (1999). Vegetation change in created emergent wetlands (1988–1996) in Connecticut (USA). *Wetlands Ecology and Management*, 7, 177–191.
- Morris, J. T., Porter, D., Neet, M., Noble, P. A., Schmidt, L., Lapine, L. A., & Jensen, J. R. (2005). Integrating LIDAR elevation data, multi-spectral imagery and neural network modeling for marsh characterization. *International Journal of Remote Sensing*, 26, 5221–5234.
- Orson, R. A. (1999). A paleoecological assessment of *Phragmites australis* in New England tidal marshes: Changes in plant community structure during the last few millennia. *Biological Invasions*, 1, 149–158.
- Pengra, B. W., Johnston, C. A., & Loveland, T. R. (2007). Mapping and invasive plant, *Phragmites australis*, in coastal wetlands using the EO-1 Hyperion hyperspectral sensor. *Remote Sensing of Environment*, 108, 74–81.
- Phinn, S. R., Stow, D. A., & Van Mouwerik, D. (1999). Remotely sensed estimates of vegetation structural characteristics in restored wetlands, southern California. *Photogrammetric Engineering and Remote Sensing*, 65, 485–493.
- Podani, J. (2000). *Introduction to the exploration of Multivariate Biological Data*. Leiden, the Netherlands: Backhuys Publishers 407 pp.
- Reed, B. C., Brown, J. F., VanderZee, D., Loveland, T. R., Merchant, J. W., & Ohlen, D. O. (1994). Measuring phenological variability from satellite imagery. *Journal of Vegetation Science*, 5, 703–714.
- Rosso, P. H., Ustin, S. L., & Hastings, A. (2006). Use of LiDAR to study changes associated with *Spartina* invasion in San Francisco Bay marshes. *Remote Sensing of Environment*, 100, 295–306.
- Sadro, S., Gastil-Buhl, M., & Melack, J. (2007). Characterizing patterns of plant distribution in a southern California salt marsh using remotely sensed topographic and hyperspectral data and local tidal fluctuations. *Remote Sensing of Environment*, 110, 226–239.
- Schmidt, K. S., & Skidmore, A. K. (2003). Spectral discrimination of vegetation types in a coastal wetland. *Remote Sensing of Environment*, 85, 92–108.
- Schmidt, K. S., Skidmore, A. K., Kloosterman, E. H., van Oosten, H., Kumar, L., & Janssen, J. A. M. (2004). Mapping coastal vegetation using an expert system and hyperspectral imagery. *Photogrammetric Engineering and Remote Sensing*, 70, 703–715.
- Shima, L. J., Anderson, R. R., & Carter, V. P. (1976). The use of aerial color infrared photography in mapping the vegetation of a freshwater marsh. *Chesapeake Science*, 17, 74–85.
- Shuman, C. S., & Ambrose, R. F. (2003). A comparison of remote sensing and ground-based methods for monitoring wetland restoration success. *Restoration Ecology*, 11, 325–333.
- Silvestri, S., Marani, M., Settle, J., Benvenuto, F., & Marani, A. (2002). Salt marsh vegetation radiometry data analysis and scaling. *Remote Sensing of Environment*, 80, 473–482.
- Singh, A. (1989). Digital change detection techniques using remotely-sensed data. *International Journal of Remote Sensing*, 10, 989–1003.
- ter Braak, C. J. F., & Šmilauer, Petr (1998). CANOCO reference manual and user's guide to Canoco for Windows: Software for Canonical Community Ordination (version 4), Centre for Biometry, Wageningen, CPRO-DLO Wageningen, the Netherlands. Microcomputer Power: Ithaca, New York 351 pp.
- Underwood, E., Ustin, S., & DiPietro, D. (2003). Mapping nonnative plants using hyperspectral imagery. *Remote Sensing of Environment*, 86, 150–161.
- Wang, C., Meneti, M., Stoll, M. -P., Belluco, E., & Marani, M. (2007). Mapping mixed vegetation communities in salt marshes using airborne spectral data. *Remote Sensing of Environment*, 107, 559–570.
- Warren, R. S., Fell, P. E., Grimsby, J. L., Buck, E. L., Rilling, G. C., & Fertik, R. A. (2001). Rates, patterns, and impacts of *Phragmites australis* expansion and effects of experimental *Phragmites* control on vegetation, macroinvertebrates, and fish within tidelands of the lower Connecticut River. *Estuaries*, 24, 90–107.
- Wooley, J. T. (1971). Reflectance and transmittance of light by leaves. *Plant Physiology*, 47, 656–662.
- Yu, Q., Gong, P., Clinton, N., Biging, G., Kelly, M., & Schirokauer, D. (2006). Object-based detailed vegetation classification with airborne high spatial resolution remote sensing imagery. *Photogrammetric Engineering and Remote Sensing*, 72, 799–811.
- Zhang, M., Ustin, S. L., Rejmankova, E., & Sanderson, E. W. (1997). Monitoring Pacific coast salt marshes using remote sensing. *Ecological Applications*, 7, 1039–1053.